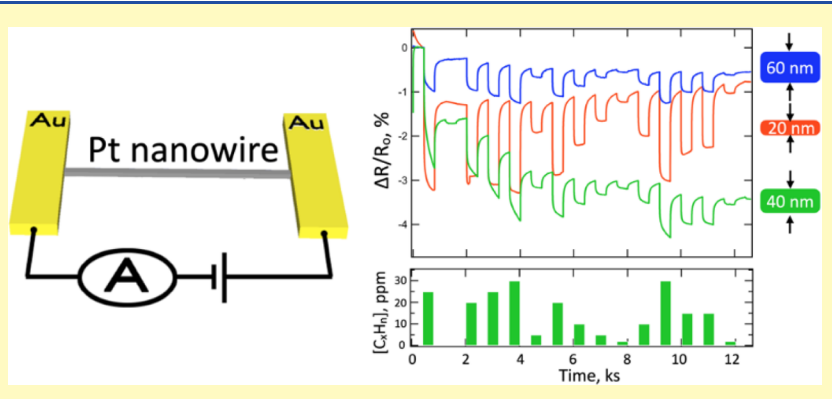


pubs.acs.org/acssensors Article

A Platinum Nanowire Sensor for Ethylene in Air

Nicholas J. Humphrey, Eric J. Choi, Nicholas P. Drago, John C. Hemminger, and Reginald M. Penner*





ABSTRACT: A single platinum nanowire (PtNW) chemiresistive sensor for ethylene gas is reported. In this application, the PtNW performs three functions: (1) Joule self-heating to a specified temperature, (2) *in situ* resistance-based temperature measurement, and (3) detection of ethylene in air as a resistance change. Ethylene gas in air is detected as a reduction in nanowire resistance by up to 4.5% for concentrations ranging from 1 to 30 ppm in an optimum NW temperature range from 630 to 660 K. This response is rapid (30–100 s), reversible, and reproducible for repetitive ethylene pulses. A threefold increase in signal amplitude is observed as the NW thickness is reduced from 60 to 20 nm, commensurate with a signal transduction mechanism involving surface electron scattering.

KEYWORDS: surface electron scattering, electrodeposition, chemiresistor, olefin, reversible

N anowires have been extensively investigated for use as transducers in chemical and biological sensors. While silicon nanowires, $^{1-3}$ metal oxide nanowires, $^{4-7}$ and carbon nanotubes $^{8-11}$ have been used as the basis of sensors for the detection of a wide variety of molecular targets, metal nanowires have been applied almost exclusively for the measurement of hydrogen gas (H_2) . In this application, palladium nanowires (PdNWs) are able to detect H_2 rapidly and reversibly because exposure to H_2 results in the spontaneous formation of electrically resistive PdH_x ($x \le 0.7$). $^{12-16}$ The spontaneous transformation of palladium metal to PdH_x in H_2 is a property unique to palladium.

Platinum nanowires (PtNWs) have also been evaluated as H_2 sensors, but a different mechanism of H_2 detection applies as compared with PdNWs.^{17,18} Unlike Pd, Pt does not form a bulk hydride phase upon exposure to H_2 ; however, a surface monohydride (Pt-H) is formed. Exposure of PtNWs to H_2 in air causes a reversible decrease in resistance that is attributed to an increase in the specularity of electron surface scattering caused by the displacement of adsorbed O_2 , H_2O , and OH from the Pt surface by Pt-H.^{17,18} These results beg the question: Could the surface scattering modality for the Pt nanowire sensing of H_2 be expanded to other gases? In this study, the investigation of ethylene detection using a PtNW is

evaluated. Like H₂, ethylene (C₂H₄) and other olefins chemisorb to Pt surfaces at or above room temperature. Ethylene is an important target for sensor development because it is a precursor for the manufacture of polymers 15 and is widely used for promoting the controlled ripening of avocadoes, bananas, and other climacteric fruits and vegetables.²⁰ Rapid, accurate, and sensitive ethylene sensors are needed because ethylene is odorless and C₂H₄/air mixtures are explosive above 3% ethylene in air. Ethylene is commonly measured using single-use Dräger tubes, 21 gas chromatography, 22 and photoacoustic spectroscopy, 23,24 but power consumption for the latter two options (1 W-2 kW) is significant. None of these sensing modalities have been adapted to handheld, portable, and continuous ethylene concentration monitoring in air, to our knowledge.²⁵ To enable real-time ethylene monitoring, several chemical sensors have been developed (Table 1). Catalytic sensors for ethylene

Received: May 5, 2023 Accepted: June 21, 2023 Published: July 7, 2023





Table 1. Performance of Some Prominent Ethylene Sensors

sensing material ^a	${\it transduction mechanism}^b$	reversibility	response time c (s)	operating temp ($^{\circ}$ C)	LOD (ppb) ^d	refs
PdCl ₂ + pH indicator	colorimetric	N	120	RT	170	28
SWCNT @PdCl2 catalytic mixture	CR	Y	n.a.	RT	500	26
Pd and rGO modified α -Fe ₂ O ₃	CR	Y	14	250	10	29
SWCNT @PdCl2 catalytic mixture	CR	Y	n.a.	40	200	27
CeO _x -SnO ₂ NPs	CR	Y	12	350	300	30
1% Pt@SnO ₂	CR	Y	n.a.	450	1000	34
SnO_2 TF	CR	Y	67	400	200,000	35
WO ₃ TF	CR	Y	58	350	200,000	35
Dräger X AM 8000	IR	Y	n.a.	RT	1,000,000	21
Dräger tube	colorimetric	N	1800	RT	200	21
single Pt nanowire	CR	Y	4.8	390	170 (est.)	this work

"SWCNT = single-walled carbon nanotubes, rGO = reduced graphene oxide, NPs = nanoparticles, TF = thin films. "CR = chemiresistive, IR = infrared spectroscopic. "The "10–90" response time, corresponding to 10–90% of the maximum signal amplitude, unless otherwise specified. "Directly measured or estimated (est.) as the [ethylene] corresponding to 3× RSD of the sensor baseline noise in the absence of ethylene.

oxidation 26,27 are both selective and sensitive but rely on a liquid-phase catalytic mixture that has not been adapted to continuous, real-time monitoring. Colorimetric sensors can be inexpensive to manufacture, but concentration measurement is less precise and reusability has not been demonstrated. While some chemiresistive sensors report rapid response times of 5–10 s, high sensitivity ($\Delta R/R_{\rm o}=4-80\%$), reusability, and high operational temperatures are required in the 300–400 °C range, at the expense of power efficiency. 29,30

EXPERIMENTAL SECTION

Reagents and Materials. Glass microscope slides (1 in. \times 1 in.) were purchased from Fisher for use as a substrate. Acetone, methanol, and nitric acid were received from Fisher. Potassium hexachloroplatinate (K_2 PtCl₆, 99% trace metal basis), potassium chloride (KCl), and hydrochloric acid (HCl) were received from Millipore Sigma. Positive photoresist (Shipley S1808) and developer (Shipley MF-319) were received from Microchem Corporation. Nickel (Ni) and gold (Au) pellets (5 N purity) were received from Kurt J. Lesker Company. Ethylene gas (100 ppm in N_2) was purchased from Linde Gas, while acetylene (100 ppm), methane (10%), and purified air (Ultra Zero Grade) were purchased from Airgas.

Platinum Nanowire Fabrication. Platinum nanowires were synthesized using the lithographically patterned nanowire electrodeposition (LPNE) process, as previously described. 18,31 Nickel films of 20, 40, or 60 nm thickness were thermally evaporated onto precleaned glass slides and thickness was monitored by a gold quartz crystal microbalance (Sigma, model SQM-160). Slides were then spin-coated with a positive photoresist layer (Shipley S1808) at 2500 rpm for 80 s (Laurell, model WS-400B-6NPP/Lite). The photoresistcoated slides were then baked in an oven (Yamato Scientific America, Inc., model DKN 600) in air for 30 min at 90 °C. After cooling to room temperature, the photoresist-covered substrates were patterned by flood exposure to ultraviolet (UV) light (Newport model 97436, iline, 365 nm, 500 W \times 2.8 s). Exposed photoresist was removed from portions of the nickel by dipping into the developer (Shipley MF-319) for 40 s, washing in Millipore water (Milli-Q $\rho > 18 \text{ M}\Omega$), and air drying. Exposed nickel was etched by submerging in a commercial nickel etchant (Alfa Aesar) for 4 min to create a trench beneath the photoresist layer. Samples were then rinsed again in Millipore water.

A one-compartment, three-electrode cell was used to electrodeposit the platinum nanowires. In a 100 mL liquid compartment, electrodes were submerged in an aqueous plating solution containing 1 mM K_2PtCl_6 and 0.1 M HCl. The etched and patterned templates were submerged and the nickel layer was connected to a potentiostat (Gamry Instruments, model G300). A 1 cm² platinum foil electrode was used as a counter electrode, and a saturated calomel electrode (SCE) was used as a reference electrode. Single PtNWs were

electrodeposited at -0.3~V~vs SCE using a 300 s chronoamperometry program. After deposition, the photoresist was removed by successive submersion in acetone, isopropyl alcohol, and water; then the nickel layer was removed by etching in a commercial nickel etchant, and the PtNW was rinsed in water.

Ethylene Sensor Fabrication and Characterization. Fourprobe contacts were fabricated using a lift-off procedure. Briefly, the nanowire-glass substrate was spin-coated with photoresist (Shipley S1808) and soft-baked. A four-probe electrode with a 50 μ m gap was patterned by a flood exposure to UV light, followed by developing in Shipley MF-319 for 40 s and washing in Millipore water. The patterned nanowire-glass substrate was plasma-oxygen cleaned (Diener, Zepto) for 10 min at 100% power to remove any remaining developed photoresist. A layer of gold (60 nm) with a chromium adhesion layer (4 nm) was evaporated onto the patterned photoresist using physical vapor deposition. The photoresist was removed by sonication in acetone for 30 s, isolating a 50 μ m segment of the nanowire. Wires were equilibrated at the highest temperature observed in the experiment (800 K) by Joule heating in ambient laboratory air until the rate of the resistance decrease was insignificant and a stable baseline was observed (≈2000 s).

Temperature Calibration. Platinum nanowires were calibrated as described previously. A programmable oven (Thermo Scientific, Lindberg/Blue M) was used to control the temperature and a multimeter (Keithley 2000) was used to acquire a series of two-point resistance measurement between 294 and 540 K—the highest temperature afforded by this oven. The resulting linear calibration curve (Figure S1) was extrapolated for higher temperatures up to 800 K.

Hydrocarbon Sensing. During a gas sensing exposure, the four-contact electrical resistivity of a PtNW sensor was monitored with a digital multimeter (Keithley Instruments, model 2000) and a source meter (Keithley Instruments, model 2400) to control the voltage and temperature applied across the nanowire. Ethylene gas, acetylene gas, or methane gas was premixed with air, N₂, or Ar (Airgas, zero grade) in a flow chamber using two mass flow controllers (MKS Inc, model 1479). This gas was pulsed onto the nanowire by switching (Parker valve, cycle time = 25 ms) between the premixed hydrocarbon/backing gas mixture and blank backing gas at a constant flow rate of 1000 SCCM. Resistivity data and instrument status were controlled by a computer interfaced with a National Instruments board (model BNC 2110). All gas sensing experiments were carried out using dry gases at ambient laboratory temperatures (20 °C).

Atomic Force Microscopy (AFM), Scanning Electron Microscopy (SEM), and Energy-Dispersive X-ray (EDX) Imaging. SEM and EDX images were collected on an FEI Magellan 400 XHR scanning electron microscope (SEM) using an accelerating voltage of 5–10 keV. An Oxford Silicon Drift Detector (80 mm²) was used to collect energy-dispersive X-ray spectroscopy (EDS) images for elemental analysis. Samples were mounted on aluminum stubs

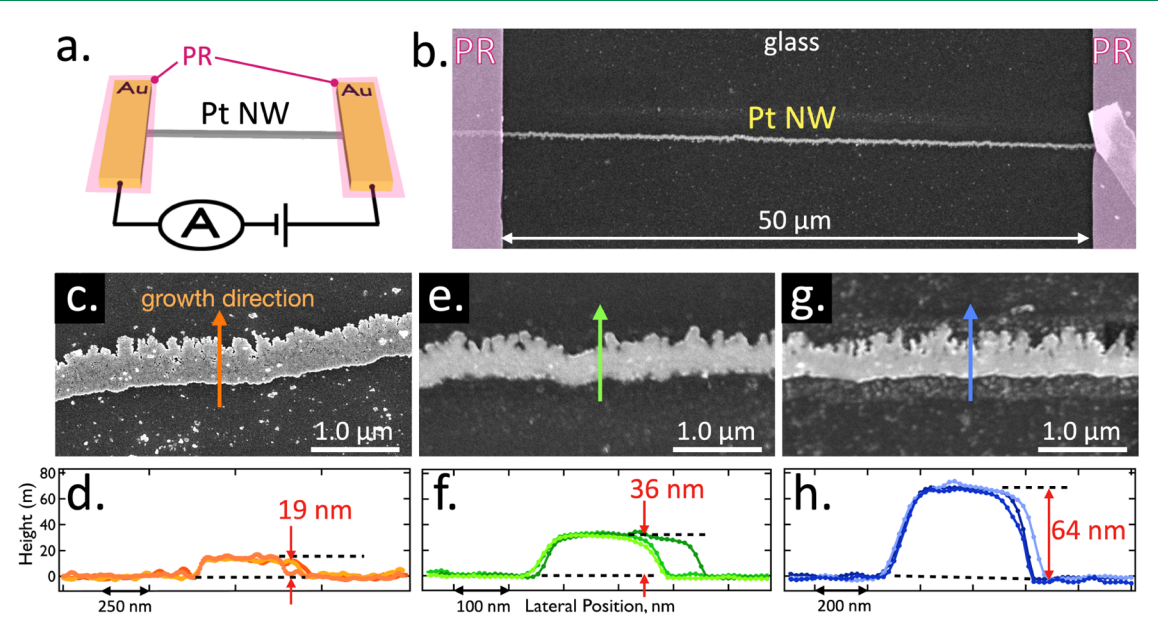


Figure 1. Single Pt nanowire sensor and PtNWs of three heights. (a) Schematic diagram of the single Pt nanowire sensors used in this study. (b) Low-magnification SEM image of a PtNW with photoresist (PR)-covered gold contacts. SEM images (c, e, g) and three AFM tip amplitude traces (d, f, h) for Pt nanowires with three heights: (d, c) $20(\pm 2)$ nm, (e, f) $40(\pm 5)$ nm, and (g, h) $60(\pm 7)$ nm. The electrodeposition growth direction in the LPNE process^{32,33} is indicated by an arrow.

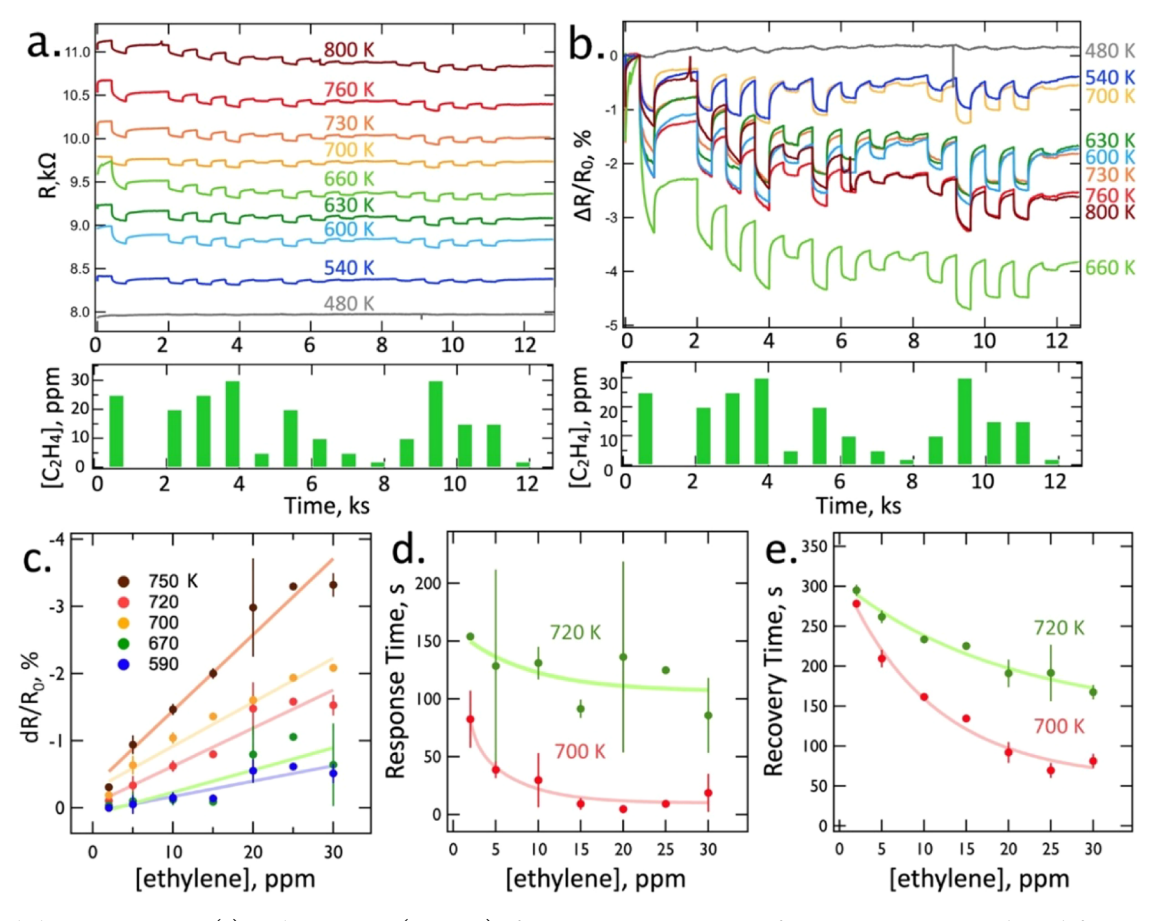


Figure 2. Ethylene sensing in air. (a) Real-time traces (200 min) of R_{NW} versus time at a series of nine temperatures as indicated, for a PtNW having dimensions of 52 \pm 1 nm (h) and 448 \pm 9 nm (w). The green bar graph at bottom indicates the program of ethylene/air pulses, with concentrations in the range from 1 to 30 ppm. (b) Same data shown in panel (a) plotted as $\Delta R/R_0$. (c) Mean values of $\Delta R/R_0$ versus $[C_2H_4]$ at five temperatures, as indicated. Error bars indicate $\pm 1\sigma$ for replicate exposures at the same PtNW sensor. (d) Response time versus $[C_2H_4]$ at two temperatures, as indicated. (e) Recovery time versus $[C_2H_4]$ at two temperatures, as indicated.

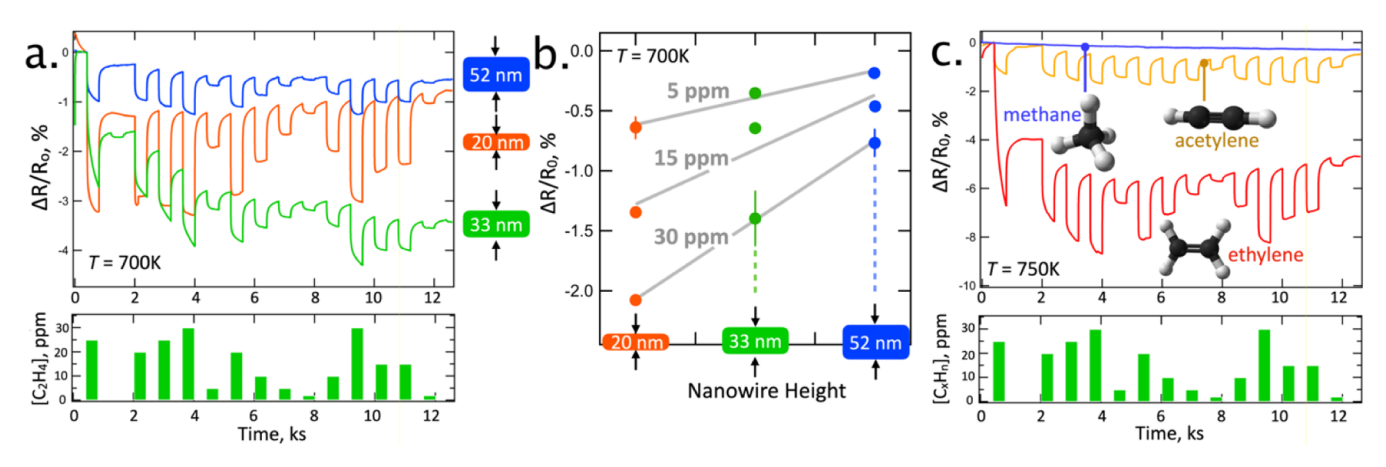


Figure 3. Influence of nanowire height and a comparison of sensitivity for three hydrocarbons. (a) $\Delta R/R_o$ versus time at 700 K for three PtNWs with heights of $20(\pm 2)$, $33(\pm 1)$, and $52(\pm 1)$ nm. Width dimensions for these nanowires are $360(\pm 20)$, $350(\pm 40)$, and $448(\pm 9)$ nm, respectively. The green graph at bottom indicates the program of applied ethylene pulses, with concentrations in the range from 1 to 30 ppm. (b) $\Delta R/R_o$ versus $[C_2H_4]$ calibration plots for the same data shown in panel (a). (c) Comparison of real-time $\Delta R/R_o$ versus time at 750 K for the same PtNW sensor detecting methane (blue), acetylene (gold), and ethylene (red), as indicated.

(Ted Pella) using a conductive carbon tape. Imaging of postexposure wires under SEM and EDX was conducted to produce Figures 2 and S3. AFM images were acquired using an Asylum Research MFP-3D microscope in contact mode with Bruker OTESPA-R3 silicone AFM tips. All images were collected in air at ambient room temperature (20 °C).

RESULTS AND DISCUSSION

Fabrication of PtNW Sensors. The PtNW ethylene sensors reported here are comprised of a single Pt nanowire chemiresistor (Figure 1a). This nanowire is prepared on a glass surface using lithographically patterned nanowire electrodeposition (LPNE) 32,33 and is 100-500 nm in width. The height or thickness of the Pt nanowire is controlled with a precision of 2-7 nm for thicknesses of 20, 40, and 60 nm (Figure 1c-f). 32,33 No effect of the larger width dimension of the nanowire on its ethylene sensing properties was observed in this study. The electrically isolated length of the nanowire, defined by two evaporated gold contacts, is 50 μ m (Figure 1b). A PtNW ethylene sensor operates by performing three functions in parallel: (1) Joule self-heating to a specified temperature from 460 to 800 K, (2) in situ resistance-based temperature measurement (temperature calibration of the NW is described in Figure S1), and (3) detection of ethylene in air at concentrations from 1 to 30 ppm as a resistance decrease relative to the resistance of the PtNW in pure air. The diminutive cross section of a Pt nanowire enables these functions to be performed using a net total power consumption of between 0.10 and 10 mW, 2-3 orders of magnitude lower than competing electrically based ethylene sensors (Table 1). This value for power consumption was calculated from the current supplied through the nanowire to measure resistance in the four-point measurement, which simultaneously heats the nanowire while monitoring its resistance and the potential drop across it.

Ethylene detection in air, N_2 , or Ar at a PtNW requires that the nanowire be heated to temperatures above 480 K. This heating is readily accomplished by thermal dissipation of the power, i^2R_{NW} (where i is the through-nanowire current), in a process called Joule self-heating. The applied voltage necessary to enable self-heating to a particular target temperature varies with R_{NW} and depends on its lateral dimensions and length. It

is therefore useful to use the nanowire itself as a resistance temperature detector (RTD) to monitor its temperature using $R_{\rm NW}$, before the exposure of the nanowire to air/ethylene mixtures. This is accomplished by first acquiring a temperature–resistance calibration for each PtNW sensor in an oven at temperatures up to 475 K (Figure S1)—a limit imposed by the ovens available in this laboratory. As expected, the $R_{\rm NW}$ versus temperature calibration of each NW is linear and the $R_{\rm NW}$ values corresponding to $T_{\rm NW} > 475$ K up to 800 K can be estimated by extrapolation (Figure S1). The uncertainty associated with this extrapolation increases with the target temperature above 475 K, as indicated in the yellow envelope shown in the plot of Figure S1 and is estimated to be ± 50 K at 750 K.

Ethylene Sensing Properties in Air. Using the described PtNWs, sensing runs were conducted with air/ethylene mixtures to determine the ethylene sensing properties of these devices. The resulting data shows temperature-dependent resistance responses that can be measured as a function of the ethylene concentration from 1 to 30 ppm (Figure 2). At or below 480 K, ethylene is not detected and no change in R_{NW} is observed across this concentration range (Figure 2a). As the PtNW is heated to 540 K, two changes are observed: First, the baseline value of R_{NW} , measured in pure air, shifts to higher R_{NW} because of the positive temperature coefficient of resistance of the platinum metal. Second, upon exposures to C₂H₄/air pulses, R_{NW} decreases reversibly, returning to the higher baseline resistance in pure air when ethylene is absent. As NW temperature is increased still further, the baseline R_{NW} in air continues to shift to higher values and the amplitude of the resistance response to ethylene, ΔR , increases across all concentrations. This increase in PtNW sensitivity to ethylene, seen more clearly in plots of $\Delta R/R_o$ versus time (Figure 2b), continues to temperatures in the range of 720-750 K. Higher temperatures up to 800 K also produce reversible ethylene sensing responses with reduced sensitivity. Plots of $\Delta R/R_0$ versus [C₂H₄] (Figure 2c) are approximately linear at all temperatures, and batch analysis of these devices (Figure S2) shows that this $\Delta R/R_0$ calibration is reproducible across devices fabricated in identical conditions.

The ability of a PtNW to discriminate $[C_2H_4]$ from 0 to 30 ppm is a capability that PtNWs do not possess for the

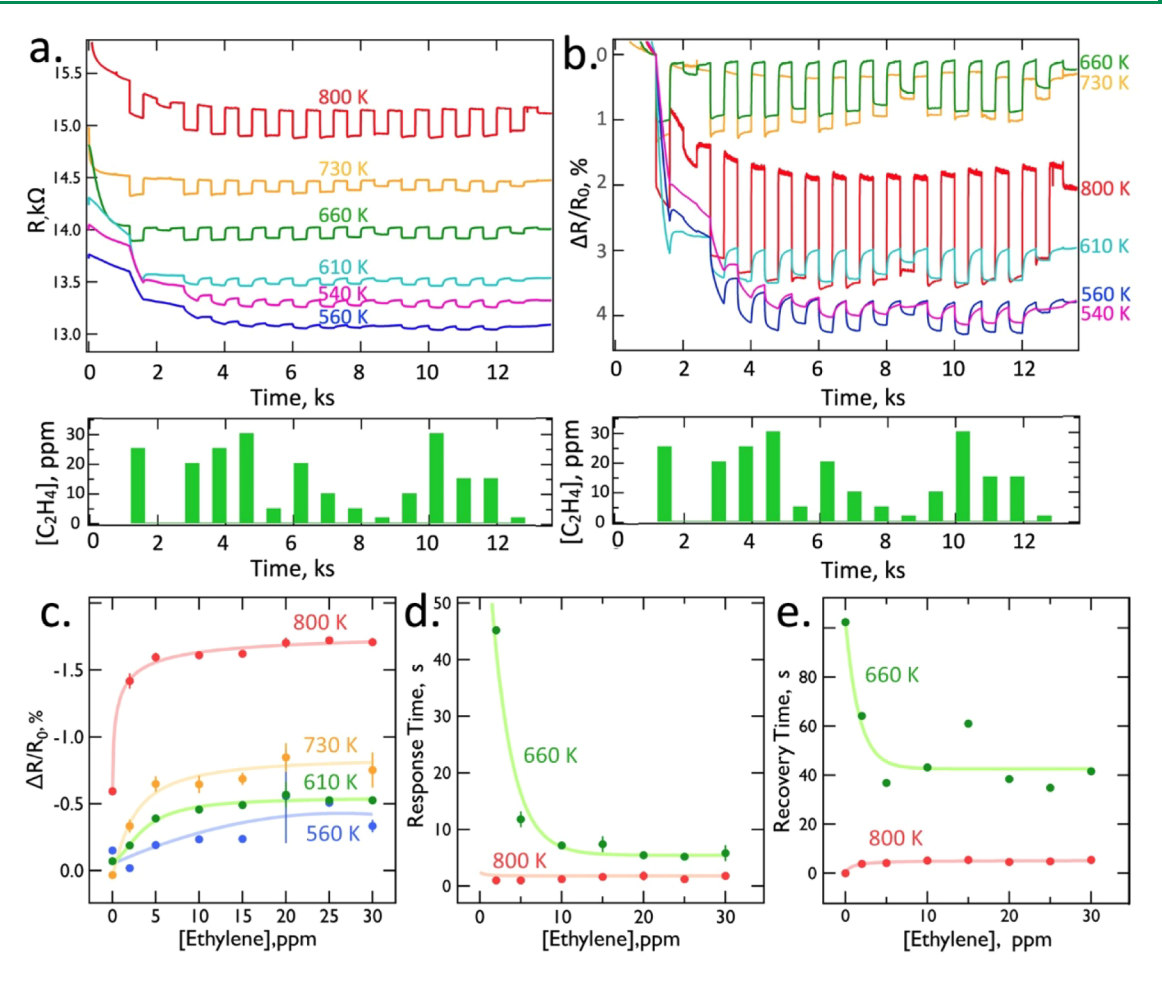


Figure 4. Ethylene sensing in N_2 . (a) R_{NW} versus time at a series of nine temperatures, as indicated, for a PtNW having dimensions of 53 \pm 1 nm (h) and 270 \pm 7 nm (w). The green bar graph at bottom indicates the program of ethylene/ N_2 pulses, with concentrations in the range from 1 to 30 ppm. (b) Same data shown in panel (a) plotted as $\Delta R/R_0$. (c) Mean values of $\Delta R/R_0$ versus $[C_2H_4]$ at four temperatures, as indicated. Error bars indicate \pm 1 σ for replicate exposures at the same PtNW sensor. (d) Response time versus $[C_2H_4]$ at two temperatures, as indicated. (e) Recovery time versus $[C_2H_4]$ at two temperatures, as indicated.

detection of H_2 in air, where H_2 concentrations ranging from ppm to 1% all produce nearly identical steady-state R_{NW} changes. The invariance of the ΔR_{NW} signal for H_2 is attributed to the saturation of Pt surfaces with a monohydride (Pt-H) layer. The invariance of the ΔR_{NW} signal for H_2 is attributed to the saturation of Pt surfaces with a monohydride (Pt-H) layer.

Surprisingly, a PtNW also exhibits faster response and recovery of R_{NW} to ethylene exposures as compared with H_2 (Figure 2d,e). For example, for 10 ppm H_2 and 550 K, the optimum temperature for H_2 response and recovery requires >1000 s independent of nanowire size. At 10 ppm ethylene and 700 K, response and recovery times of 29 and 90 s are obtained, respectively. The measurement of $[C_2H_4]$ below 1 ppm was not attempted in this study, but a limit of detection of 100-200 ppb is estimated based upon the $[C_2H_4]$ value corresponding to 3(RSD) of the PtNW sensor background in air.

In addition to ethylene, PtNWs also show a resistance response upon exposure to other olefins such as acetylene, but some molecular class selectivity is observed in a comparison of acetylene, ethylene, and methane at 750 K (Figure 3c). Here, larger resistance responses are observed for ethylene *versus* acetylene at the same PtNW while no response is observed for methane, an alkane. A response time minimum of 4.8 s was recorded at 20 ppm, which is also the fastest reported response time for an ethylene sensor in air to our knowledge (Table 1).

What is the mechanism responsible for the reversible reduction in R_{NW} caused by exposure to ethylene? A transduction mechanism involving the adsorbate-modulated electron surface scattering is implicated by two observations.³⁶ First, the sensitivity of PtNWs to ethylene increases with decreasing nanowire height—the smallest dimension of the nanowires investigated here (Figure 1). A comparison of PtNWs with heights of $20(\pm 2)$, $40(\pm 3)$, and $60(\pm 4)$ nm (Figure 3a) shows the amplitude of $\Delta R/R_0$ increases by a factor of ≈2.5 over this height range. Second, the magnitudes of the observed $\Delta R/R_o$ responses, ranging from 1 to 5%, are also in the range expected for this mechanism. In adsorbatemodulated electron surface scattering, a resistance change for the NW is produced by a change in the specularity of electron surface scattering, p, at nanowire surfaces (0mediated by adsorbate species on the NW surface. The resistivity of a Pt metal nanowire, ρ , is related to the electron mean free path, λ_{Pt} and the smallest lateral dimension of the PtNW, d^{37-39}

$$\rho = \rho_0 \left\{ 1 + \frac{3}{8} (1 - p) \frac{\lambda_{\text{Pt}}}{d} \right\}$$
 (1)

The specular surface scattering of electrons, in which the momentum of conduction electrons is conserved in each ACS Sensors pubs.acs.org/acssensors Article

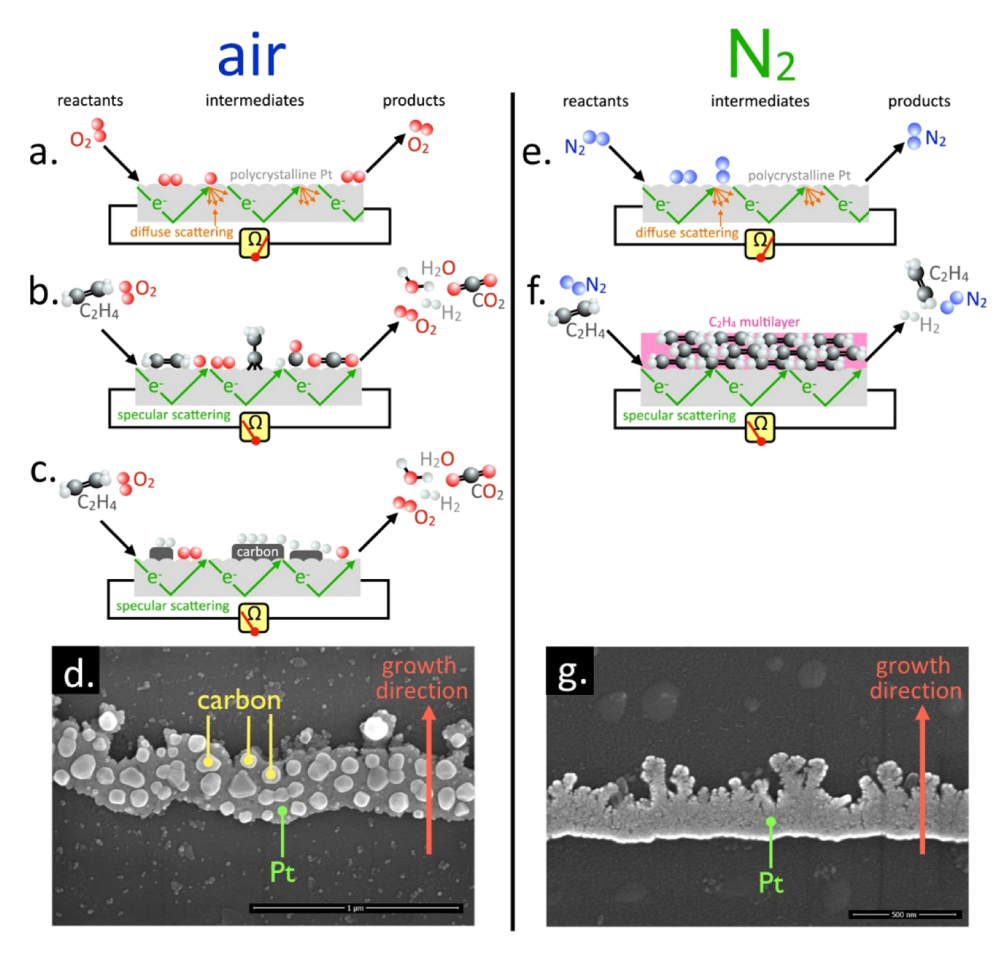


Figure 5. Proposed mechanisms for ethylene detection (a–c and e, f) and SEM images of PtNW sensors in air (d) and N_2 (g). (a) In an air ambient, O_2 will physisorb, chemisorb, and dissociate. O_2 will desorb from this surface. (b) In ethylene/air mixtures, the combustion of ethylene will occur producing CO_2 and H_2O as primary products and H_2 , CO_2 , and CO_2 as minor products. Coverage of the Pt surface by several intermediates produces specular scattering of electrons at the Pt surface. (c) For T > 700 K, repetitive ethylene exposures cause the irreversible formation of carbon particles on the Pt surface, but these particles do not significantly degrade the detection of ethylene. (d) SEM image showing a PtNW after ethylene testing in air at 700 K. (e) In a N_2 or Ar ambient, these gases do not significantly adsorb to the Pt surface. (f) In N_2 or Ar mixtures, high fluxes of C_2H_4 result in the physisorption of molecular C_2H_4 layers producing specular scattering at the Pt surface. It is proposed that ethylene molecular layers reversibly form for $[C_2H_4] > 1$ ppm and rapidly desorb in pure N_2 or Ar. (g) SEM image showing a PtNW after ethylene testing in N_2 at 700 K.

scattering event, is characterized by p=1, while a diffuse scattering event that dissipates momentum has p=0. The largest possible change in ρ corresponding to a transition from p=0 to p=1.0 is given by p=0

$$\frac{\Delta \rho}{\rho_0} = \frac{3}{16} \frac{\lambda_{\text{Pt}}}{d} \tag{2}$$

Using $\lambda_{\rm Pt}\approx 12$ nm, ⁴⁰ eq 2 predicts a maximum $\Delta\rho/\rho_o$ ranging from 4% (d=60 nm) to 11% (20 nm), spanning the range of nanowire thicknesses explored here. Consistent with this prediction, the observed values of $\Delta\rho/\rho_o$ range from 1% (d=60 nm) to 4.5% (20 nm).

The ability to predict p for a particular adsorbate—metal system is not yet possible experimentally or theoretically, to our knowledge. In the experiments described here, the value of p increases during exposure to ethylene mixtures—with air, N_2 , and Ar—relative to when ethylene is absent. We speculate that the reversible change in p is attributed to a change in the identities and coverages of the adsorbates present on the Pt surface. The ethylene/platinum system has been extensively studied both in ultrahigh vacuum^{41–43} and at ambient

pressure 44,45 providing a basis for hypotheses, discussed below, that account for the mechanisms operating in ethylene sensing experiments conducted in air. These hypotheses are also informed by experiments involving ethylene sensing at PtNWs in N₂ (Figure 4) and Ar (Figure S3) that were conducted to advance our understanding of the mechanisms operating in air.

A universal observation in every ethylene sensing experiment is a rapid decrease in the PtNW resistance that coincides with heating and exposure to a highly purified stream of air, N_2 , or Ar (Figures 2b, 3a, 4b, and S2). Since every PtNW sensor is exposed to laboratory air, its Pt surfaces are covered with hydrocarbons, adsorbed water, and other air-borne contaminants. The observed decrease in R_{NW} is attributed to catalytic "cleaning" of the Pt surface in these purified gases at elevated temperatures. Equilibration of the hot NW with air is expected to induce desorption and/or oxidation of volatile contaminants and the chemisorption of O_2 produces a surface oxide, Pt-O (Figure 5a). The lower resistance produced during this initial cleaning process will equal the high resistance state of the PtNW in subsequent ethylene sensing experiments. The

ACS Sensors pubs.acs.org/acssensors Article

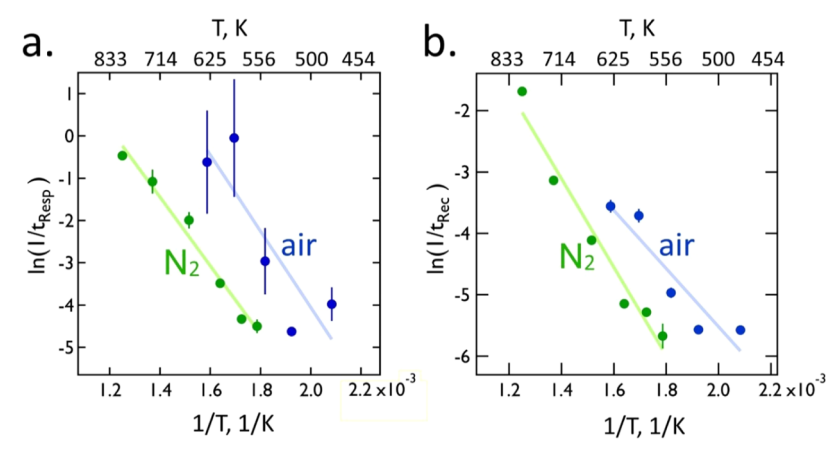


Figure 6. Arrhenius plots for (a) response and (b) recovery to ethylene exposure (at 15 ppm) for PtNWs in air (blue) and N_2 (green). The response and recovery rates (units: s^{-1}) are estimated as $1/t_{resp}$ and $1/t_{resp}$ respectively. Apparent activation energies, $E_{q,app}$, for a response are (a), $18(\pm 6)$ kcal/mol (air) and $16.1(\pm 0.8)$ kcal/mol (N_2), and for recovery: (b), $9(\pm 2)$ kcal/mol (air) and $14.3(\pm 0.9)$ kcal/mol (N_2). Nanowire dimensions are (air) $52.0(\pm 0.7)$ nm (h) and $448(\pm 9)$ nm (w), and (N_2) $53(\pm 1)$ nm (h) and $270(\pm 7)$ nm (w).

rational for this is the fact that chemisorbed oxygen is a promoter of diffuse electron surface scattering. A single oxide monolayer on copper, for example, has been shown to reduce p to zero.³⁷ It is proposed that chemisorbed oxygen (Pt = O), Pt-OH, and water are responsible for the high resistance state seen for PtNWs in air.

The low resistance state associated with the presence of ethylene is produced by the presence on the Pt surface of intermediates involved in ethylene combustion. At temperatures above 370 K, ethylene undergoes spontaneous combustion producing CO_2 and water⁴⁴

$$C_2H_4 + 3O_2 \rightarrow 2H_2O + 2CO_2$$
 (3)

The apparent activation energy, $E_{a,app}$, for eq 3 in air is 14-17 kcal/mol44 at the pressures employed in this study, in reasonable agreement with the value of $E_{a,app} = 18(\pm 6)$ kcal/ mol obtained from an analysis of response rates measured in air (Figure 6a). The low resistance state observed for air/ ethylene mixtures likely derives from the presence of chemisorbed intermediates involved in combustion, including Pt-H, Pt-O, CO, ethylidyne (C_2H_3) , and other C_xH_y where y/x < 2 (Figure 5b). It is proposed that this ensemble of intermediates displaces oxygen on the Pt surface, increasing p relative to its value in pure air and thereby reducing R_{NW} . At high temperatures (450-770 K), adsorbed ethylene undergoes conversion first to ethylidyne (Pt–C–CH $_3$) and then to "carbidic" carbon (C_xH_y) . ^{46,47} Experimental data for the conversion of ethylene to ethylidyne is observed with $E_{a,app}$ = 18 kcal/mol, 43 which matches our experimental $E_{a,app}$ derived from the response time (Figure 6a), suggesting that ethylidyne formation could be the process limiting the response time of the sensor. In ultrahigh vacuum (UHV) experiments,41 continued heating is known to cause further dehydrogenation of ethylidene-producing carbidic carbon and eventually graphite particles at 800 K (Figure 5c). Identification of these particles in EDX mode confirms the carbonaceous composition of these particles (Figure S4). Faceted islands, similar to those of graphite islands seen on Pt(111) in UHV, are also observed by SEM on PtNW sensors after exposures to ethylene at temperatures in this range (Figure 5d). The recovery time in air is also thermally activated with $E_{a,app}$ = $9(\pm 2)$ kcal/mol (Figure 6b). Physisorbed CO_2 on clean platinum has a heat of adsorption of 9.6 kcal/mol, 48,49

consistent with the $E_{a,app}$ values measured here for recovery in air. Therefore, in air, it is tentatively proposed that the recovery in resistance after an ethylene exposure is limited by the oxidation of carbonaceous particles that produce adsorbed CO_2 as a product.

Ethylene Sensing Properties in Nitrogen and Argon. PtNWs are also able to detect ethylene in N₂ and Ar backgrounds (Figures 4 and S2, respectively), but two marked differences are observed: First, responses in these inert gases are more rapid and more reversible (Figure 4a,b). Response times (Figure 4d) and recovery times (Figure 4e) are both faster than in air. Second, saturation behavior is seen as a function of ethylene concentration above 5 ppm. The maximum $\Delta R/R_o$ corresponding to 30 ppm ethylene is also smaller than observed in air, with $\Delta R/R_{\rm o} \approx 1.5\%$ versus the air value of 3.5% at NWs with 20 nm thickness. Beyond these two differences, a mechanism accounting for ethylene detection must also consider that, in contrast to O_2 , neither $N_2^{50,51}$ nor Ar⁵² adsorbs in the temperature range explored here, and ethylene oxidation cannot occur in the absence of oxygen. However, dehydrogenation of the ethylene-producing Pt-H, ethylidyne (C_2H_3), and other C_xH_y (y/x < 2) remains possible, and likely, as in air. Consistent with this expectation, an apparent activation energy of $16.1(\pm 0.8)$ kcal/mol is obtained from response times measured in N_2 (Figure 5). This value is close to the 18 kcal/mol barrier predicted⁴³ for the dehydrogenation of chemisorbed ethylene to form ethylidyne $(Pt-C-CH_3)$

$$Pt - CH2 - CH2 - Pt \rightleftharpoons Pt - C - CH3 + Pt - H$$
(4)

The presence of ethylidyne and other chemisorbed intermediates produced by dehydrogenation cannot account for the rapid and reversible modulation of R_{NW} by ethylene seen in these experiments (Figure 5).

A key question is: What chemical state of the Pt surface could be responsible for the low resistance state seen in N_2 and Ar upon exposure to ethylene? A model consistent with these observations is the reversible formation of a physisorbed molecular ethylene of perhaps one to two monolayers on the PtNW in both N_2 and Ar (Figure 5f). A highly fluctional molecular layer could be expected to condense because of the significant fluxes of ethylene at the PtNW surfaces, estimated

ACS Sensors pubs.acs.org/acssensors Article

to be 800-2200 ML/s at 1-30 ppm ethylene. Since oxidation/combustion is not possible, the Pt surface can be expected to be covered by dehydrogenated intermediates that block surface sites and impede continued dehydrogenation to carbon and graphite, as observed in air. Onto this surface, a few monolayers of molecular ethylene might condense when it is present in the gas phase and then rapidly desorb when the ethylene flux is reduced to zero. This mechanism is supported by the fact that the resistance change does not depend on the concentration of ethylene in these experiments; the low resistance state of the wire is achieved upon saturation and is identical across low and high ethylene concentrations. A hypothesis is that such an ethylene molecular layer could account for the low R_{NW} state observed in the presence of ethylene, and removal of these molecular layers in the absence of ethylene then produces the higher R_{NW} state seen in the absence of ethylene. A puzzling and unresolved observation is that the desorption of molecular ethylene from such molecular layers would likely be very weakly activated, with $E_{a,app} \approx 1-3$ kcal/mol,⁵³ a number much lower than is deduced from measurements of recovery times in this study. If partial dehydrogenation occurs in the N2 and Ar ambients, then this larger barrier could be explained by the platinum-bound ethylidene and ethylidyne rehydrogenating and desorbing as ethylene.

CONCLUSIONS

In summary, the detection of ethylene in air at ppm concentrations has been accomplished using chemiresistors consisting of single Pt nanowires. Despite its simplicity, temperature control of the PtNW transducer is readily accomplished using Joule self-heating to an optimal temperature of ≈660 K that is measured using the Pt nanowire itself. Under these conditions, ethylene detection is reversible and rapid with response times in the 4–75 s. The recovery of R_{NW} from ethylene exposure to the air baseline occurs in 50–300 s. As in prior investigations involving the detection of H2 using a PtNW, 17,18 the decrease in R_{NW} by ethylene is attributed to an increase in the specularity parameter, p, in the presence of ethylene, possibly caused by the removal of oxygen from the Pt surface during the ethylene combustion process. In N2 and Ar ambients where oxidation/combustion cannot occur, PtNWs respond and recover much more rapidly to ethylene exposures, but a weaker concentration dependence is reproducibly observed, characterized by saturation of the R_{NW} at ethylene concentrations below 10 ppm. It is suggested that these rapid, reversible R_{NW} responses in N_2 and Ar may be caused by the reversible condensation and desorption of molecular ethylene layers on the nanowire surface.

ASSOCIATED CONTENT

Supporting Information

The Supporting Information is available free of charge at https://pubs.acs.org/doi/10.1021/acssensors.3c00885.

PtNW thermal calibration process (Figure S1); batch analysis of PtNWs sensitivity toward ethylene (Figure S2); ethylene sensing in three backing gasses (Figure S3); and SEM and EDS images of a carbon-particle-coated platinum nanowire (Figure S4) (PDF)

AUTHOR INFORMATION

Corresponding Author

Reginald M. Penner — Department of Chemistry, University of California, Irvine, California 92697-2025, United States; orcid.org/0000-0003-2831-3028; Email: rmpenner@uci.edu

Authors

Nicholas J. Humphrey — Department of Chemistry, University of California, Irvine, California 92697-2025, United States; orcid.org/0000-0002-3246-2870

Eric J. Choi – Department of Chemistry, University of California, Irvine, California 92697-2025, United States; orcid.org/0000-0003-3287-1284

Nicholas P. Drago — Department of Chemistry, University of California, Irvine, California 92697-2025, United States; orcid.org/0000-0002-3790-552X

John C. Hemminger — Department of Chemistry, University of California, Irvine, California 92697-2025, United States; orcid.org/0000-0003-2467-6630

Complete contact information is available at: https://pubs.acs.org/10.1021/acssensors.3c00885

Notes

The authors declare no competing financial interest.

ACKNOWLEDGMENTS

The authors acknowledge the financial support of this work by the National Science Foundation (CBET-2149631 and CHE-2201042). SEM and EDX data were acquired in the Irvine Materials Research Institute (IMRI) at the University of California, Irvine.

REFERENCES

- (1) Peng, F.; Su, Y.; Zhong, Y.; Fan, C.; Lee, S.-T.; He, Y. Silicon Nanomaterials Platform for Bioimaging, Biosensing, and Cancer Therapy. *Acc. Chem. Res.* **2014**, *47*, 612–623.
- (2) Wang, Y.; Wang, T.; Da, P.; Xu, M.; Wu, H.; Zheng, G. Silicon Nanowires for Biosensing, Energy Storage, and Conversion. *Adv. Mater.* **2013**, 25, 5177–5195.
- (3) Shehada, N.; Brönstrup, G.; Funka, K.; Christiansen, S.; Leja, M.; Haick, H. Ultrasensitive Silicon Nanowire for Real-World Gas Sensing: Noninvasive Diagnosis of Cancer from Breath Volatolome. *Nano Lett.* **2015**, *15*, 1288–1295.
- (4) Comini, E. Integration of Metal Oxide Nanowires in Flexible Gas Sensing Devices. *Sensors* **2013**, *13*, 10659–10673.
- (5) Cho, S.-Y.; Yoo, H.-W.; Kim, J. Y.; Jung, W.-B.; Jin, M. L.; Kim, J.-S.; Jeon, H.-J.; Jung, H.-T. High-Resolution p-Type Metal Oxide Semiconductor Nanowire Array as an Ultrasensitive Sensor for Volatile Organic Compounds. *Nano Lett.* **2016**, *16*, 4508–4515.
- (6) Ramgir, N.; Datta, N.; Kaur, M.; Kailasaganapathi, S.; Debnath, A. K.; Aswal, D. K.; Gupta, S. K. Metal Oxide Nanowires for Chemiresistive Gas Sensors: Issues, Challenges and Prospects. *Colloids Surf., A* **2013**, 439, 101–116.
- (7) Dey, A. Semiconductor Metal Oxide Gas Sensors: A Review. *Mater. Sci. Eng. B* **2018**, 229, 206–217.
- (8) Han, T.; Nag, A.; Mukhopadhyay, S. C.; Xu, Y. Carbon Nanotubes and Its Gas-Sensing Applications: A Review. *Sens. Actuators, A* **2019**, 291, 107–143.
- (9) Ziegler, J. M.; Andoni, I.; Choi, E. J.; Fang, L.; Flores-Zuleta, H.; Humphrey, N. J.; Kim, D. H.; Shin, J.; Youn, H.; Penner, R. M. Sensors Based Upon Nanowires, Nanotubes, and Nanoribbons: 2016-2020. *Anal. Chem.* **2021**, *93*, 124–166.

- (10) de Volder, M. F. L.; Tawfick, S. H.; Baughman, R. H.; Hart, A. J. Carbon Nanotubes: Present and Future Commercial Applications. *Science* **2013**, *339*, 535–539.
- (11) Norizan, M. N.; Moklis, M. H.; Demon, S. Z. N.; Halim, N. A.; Samsuri, A.; Mohamad, I. S.; Knight, V. F.; Abdullah, N. Carbon Nanotubes: Functionalisation and Their Application in Chemical Sensors. *RSC Adv.* **2020**, *10*, 43704–43732.
- (12) Li, X.; Liu, Y.; Hemminger, J. C.; Penner, R. M. Catalytically Activated Palladium@Platinum Nanowires for Accelerated Hydrogen Gas Detection. ACS Nano 2015, 9, 3215–3225.
- (13) Yang, F.; Taggart, D. K.; Penner, R. M. Fast, Sensitive Hydrogen Gas Detection Using Single Palladium Nanowires That Resist Fracture. *Nano Lett.* **2009**, *9*, 2177–2182.
- (14) Yang, F.; Taggart, D. K.; Penner, R. M. Joule Heating a Palladium Nanowire Sensor for Accelerated Response and Recovery to Hydrogen Gas. *Small* **2010**, *6*, 1422–1429.
- (15) Koo, W. T.; Cho, H. J.; Kim, D. H.; Kim, Y. H.; Shin, H.; Penner, R. M.; Kim, I. D. Chemiresistive Hydrogen Sensors: Fundamentals, Recent Advances, and Challenges. *ACS Nano* **2020**, *14*, 14284–14322.
- (16) Jung, D.; Han, M.; Lee, G. S. Fast-Response Room Temperature Hydrogen Gas Sensors Using Platinum-Coated Spin-Capable Carbon Nanotubes. ACS Appl. Mater. Interfaces 2015, 7, 3050–3057.
- (17) Yoo, H.-W.; Cho, S.-Y.; Jeon, H.-J.; Jung, H.-T. Well-Defined and High Resolution Pt Nanowire Arrays for a High Performance Hydrogen Sensor by a Surface Scattering Phenomenon. *Anal. Chem.* **2015**, *87*, 1480–1484.
- (18) Yang, F.; Donavan, K. C.; Kung, S. C.; Penner, R. M. The Surface Scattering-Based Detection of Hydrogen in Air Using a Platinum Nanowire. *Nano Lett.* **2012**, *12*, 2924–2930.
- (19) Patel, R. M. Polyethylene. In *Multilayer Flexible Packaging*, 2nd ed.; William Andrew Publishing, 2016; pp 17–34.
- (20) Iqbal, N.; Khan, N. A.; Ferrante, A.; Trivellini, A.; Francini, A.; Khan, M. I. R. Ethylene Role in Plant Growth, Development and Senescence: Interaction with Other Phytohormones. *Front. Plant Sci.* **2017**, *08*, No. 475.
- (21) Dräger Inc. Dräger tubes.
- (22) Zaidi, N. A.; Tahir, M. W.; Vellekoop, M. J.; Lang, W. A Gas Chromatographic System for the Detection of Ethylene Gas Using Ambient Air as a Carrier Gas. *Sensors* **2017**, *17*, No. 2283.
- (23) De Gouw, J. A.; Te Lintel Hekkert, S.; Mellqvist, J.; Warneke, C.; Atlas, E. L.; Fehsenfeld, F. C.; Fried, A.; Frost, G. J.; Harren, F. J. M.; Holloway, J. S.; Lefer, B.; Lueb, R.; Meagher, J. F.; Parrish, D. D.; Patel, M.; Pope, L.; Richter, D.; Rivera, C.; Ryerson, T. B.; Samuelsson, J.; Walega, J.; Washenfelder, R. A.; Weibring, P.; Zhu, X. Airborne Measurements of Ethene from Industrial Sources Using Laser Photo-Acoustic Spectroscopy. *Environ. Sci. Technol.* 2009, 43, 2437—2442
- (24) Ba, T. N.; Triki, M.; Desbrosses, G.; Vicet, A. Quartz-Enhanced Photoacoustic Spectroscopy Sensor for Ethylene Detection with a 3.32 μ m Distributed Feedback Laser Diode. *Rev. Sci. Instrum.* **2015**, 86, No. 023111.
- (25) Cristescu, S. M.; Mandon, J.; Arslanov, D.; De Pessemier, J.; Hermans, C.; Harren, F. J. M. Current Methods for Detecting Ethylene in Plants. *Ann. Bot.* **2013**, *111*, 347–360.
- (26) Fong, D.; Luo, S. X.; Andre, R. S.; Swager, T. M. Trace Ethylene Sensing via Wacker Oxidation. *ACS Cent. Sci.* **2020**, *6*, 507–512.
- (27) Ishihara, S.; Bahuguna, A.; Kumar, S.; Krishnan, V.; Labuta, J.; Nakanishi, T.; Tanaka, T.; Kataura, H.; Kon, Y.; Hong, D. Cascade Reaction-Based Chemiresistive Array for Ethylene Sensing. *ACS Sens.* **2020**, *5*, 1405–1410.
- (28) Li, Z.; Suslick, K. S. Colorimetric Sensor Array for Monitoring CO and Ethylene. *Anal. Chem.* **2019**, *91*, 797–802.
- (29) Li, B.; Li, M.; Meng, F.; Liu, J. Highly Sensitive Ethylene Sensors Using Pd Nanoparticles and RGO Modified Flower-like Hierarchical Porous α -Fe2O3. *Sensor. Actuators, B* **2019**, 290, 396–405.

- (30) Leangtanom, P.; Wisitsoraat, A.; Jaruwongrungsee, K.; Chanlek, N.; Phanichphant, S.; Kruefu, V. Highly Sensitive and Selective Ethylene Gas Sensors Based on CeOx-SnO2 Nanocomposites Prepared by a Co-Precipitation Method. *Mater. Chem. Phys.* **2020**, 254. No. 123540.
- (31) Yang, F.; Kung, S. C.; Cheng, M.; Hemminger, J. C.; Penner, R. M. Smaller Is Faster and More Sensitive: The Effect of Wire Size on the Detection of Hydrogen by Single Palladium Nanowires. *ACS Nano* **2010**, *4*, 5233–5244.
- (32) Menke, E. J.; Thompson, M. A.; Xiang, C.; Yang, L. C.; Penner, R. M. Lithographically Patterned Nanowire Electrodeposition. *Nat. Mater.* **2006**, *5*, 914–919.
- (33) Xiang, C.; Kung, S.-C.; Taggart, D. K.; Yang, F.; Thompson, M. A.; Güell, A. G.; Yang, Y.; Penner, R. M. Lithographically Patterned Nanowire Electrodeposition: A Method for Patterning Electrically Continuous Metal Nanowires on Dielectrics. *ACS Nano* **2008**, *2*, 1939–1949.
- (34) Ivanov, P.; Llobet, E.; Vergara, A.; Stankova, M.; Vilanova, X.; Hubalek, J.; Gracia, I.; Cané, C.; Correig, X. Towards a Micro-System for Monitoring Ethylene in Warehouses. *Sens. Actuators, B* **2005**, 111–112, 63–70.
- (35) Krivec, M.; Leitner, R.; Waldner, R.; Gostner, J.; Überall, F. In The Effect of Sensor Temperature and MOx Layer Thickness on the Sensitivity of SnO₂ and WO₃ -Based Chemiresistive Sensors to Ethylene Gas, Proceedings SPIE; SPIE, 2015.
- (36) Tobin, R. G. Mechanisms of Adsorbate-Induced Surface Resistivity—Experimental and Theoretical Developments. *Surf. Sci.* **2002**, *502*–*503*, 374–387.
- (37) Wißmann, P. The Electrical Resistivity of Pure and Gas Covered Metal Films. In *Surface Physics*; Springer, 1975; Vol. 77, pp 1–96.
- (38) Fuchs, K. The Conductivity of Thin Metallic Films According to the Electron Theory of Metals. *Math. Proc. Cambridge Philos. Soc.* **1938**, 34, 100–108.
- (39) Sondheimer, E. H. The Mean Free Path of Electrons in Metals. *Adv. Phys.* **1952**, *1*, 1–42.
- (40) Fischer, G.; Hoffmann, H.; Vancea, J. Mean Free Path and Density of Conductance Electrons in Platinum Determined by the Size Effect in Extremely Thin Films. *Phys. Rev. B* **1980**, *22*, 6065–6073.
- (41) Johánek, V.; De La Ree, A. B.; Hemminger, J. C. Scanning Tunneling Microscopy Investigation of the Conversion of Ethylene to Carbon Clusters and Graphite on Pt(111). *J. Phys. Chem. C* **2009**, 113, 4441–4444.
- (42) Erley, W.; Li, Y.; Land, D. P.; Hemminger, J. C. The Conversion of Ethylene to Ethylidyne on Pt(111): Non-First Order Kinetics and Ensemble Effects. *Surf. Sci.* **1994**, *301*, 177–196.
- (43) Carter, E. A.; Koel, B. E. A Method for Estimating Surface Reaction Energetics: Application to the Mechanism of Ethylene Decomposition on Pt(111). *Surf. Sci.* **1990**, *226*, 339–357.
- (44) Ackelid, U.; Olsson, L.; Petersson, L.-G. Ethylene Oxidation on Polycrystalline Platinum over Eight Orders of Magnitude in Ethylene Pressure: A Kinetic Study in the Viscous Pressure Regime. *J. Catal.* **1996**, *161*, 143–155.
- (45) Ackelid, U.; Wallenberg, L. R.; Petersson, L.-G. Kinetics of Ethylene Oxidation on Plane Pt/SiO2 Catalysts in the Viscous Pressure Regime: Evidence of Support Activity. *Catal. Lett.* **1996**, *39*, 129–139.
- (46) Land, T. A.; Michely, T.; Behm, R. J.; Hemminger, J. C.; Comsa, G. Direct Observation of Surface Reactions by Scanning Tunneling Microscopy: Ethylene→Ethylidyne → Carbon Particles → Graphite on Pt(111). *J. Chem. Phys.* **1992**, *97*, *6774*−*6783*.
- (47) Pettiette-Hall, C. L.; Land, D. P.; McIver, R. T.; Hemminger, J. C. Kinetics of the Ethylene to Ethylidyne Conversion Reaction on Pt(111) Studied by Laser-Induced Thermal Desorption/Fourier Transform Mass Spectrometry. *J. Phys. Chem.* **1990**, *94*, 1948–1953. (48) Liu, Z. M.; Zhou, Y.; Solymosi, F.; White, J. M. Spectroscopic
- Study of K-Induced Activation of CO2 on Pt(111. Surf. Sci. 1991, 245, 289–304.

- (49) Norton, P. R. An Investigation of the Adsorption of Oxygen and Oxygen Containing Species on Platinum by Photoelectron Spectroscopy. Surf. Sci. 1975, 47, 98-114.
- (50) Arumainayagam, C. R.; Tripa, C. E.; Xu, J.; Yates, J. T. IR Spectroscopy of Adsorbed Dinitrogen: A Sensitive Probe of Defect Sites on Pt(111. Surf. Sci. 1996, 360, 121-127.
- (51) Tripa, C. E.; Zubkov, T. S.; Yates, J. T.; Mavrikakis, M.; Nørskov, J. K. Molecular N2 Chemisorption—Specific Adsorption on Step Defect Sites on Pt Surfaces. J. Chem. Phys. 1999, 111, 8651-8658.
- (52) Tully, J. C. Dynamics of Gas-Surface Interactions: Thermal Desorption of Ar and Xe from Platinum. Surf. Sci. 1981, 111, 461-
- (53) Acree, W.; Chickos, J. S. Phase Transition Enthalpy Measurements of Organic and Organometallic Compounds. Sublimation, Vaporization and Fusion Enthalpies From 1880 to 2010. J. Phys. Chem. Ref. Data 2010, 39, No. 043101.

□ Recommended by ACS

Alkyl-Chain-Length and Temperature Dependencies of Sensor Responses to Aliphatic Alcohols in Nanostructured **Pt-Based Sensors**

Yusuke Hamanaka, Ken Uchida, et al.

SEPTEMBER 11, 2023

ACS APPLIED NANO MATERIALS

Pt-Doped HfS, Monolayer as a Novel Sensor and Scavenger for Dissolved Gases (H2, CO2, CH4, and C2H2) in Transformer Oil: A Density Functional Theory Study

Long Huang, Qu Zhou, et al.

AUGUST 29, 2023

LANGMUIR

READ **C**

ZnO Nanorod-Immobilized Pt Single-Atoms as an **Ultrasensitive Sensor for Triethylamine Detection**

Lingyue Liu, Shourong Zheng, et al.

FEBRUARY 24, 2023

ACS APPLIED MATERIALS & INTERFACES

READ 🗹

2D PtSe₂ Enabled Wireless Wearable Gas Monitoring Circuits with Distinctive Strain-Enhanced Performance

Zhehan Wang, Li Tao, et al.

JUNE 09, 2023

ACS NANO

READ

Get More Suggestions >